Supplement of Atmos. Chem. Phys., 26, 6909–6927, 2026
https://doi.org/10.5194/acp-26-6909-2026-supplement

Atmospheric Chemistry and Physics
Open Access
EGU

Supplement of

From cylinder to city: how recondensation-induced nucleation in vehicle exhaust shapes urban aerosol number

Jen-Ping Chen et al.

Correspondence to: Jen-Ping Chen (jpchen@ntu.edu.tw)

This section contains supplementary figures that provide additional details on the observational datasets, model configuration, and model–observation comparisons that support the analyses presented in the main text.

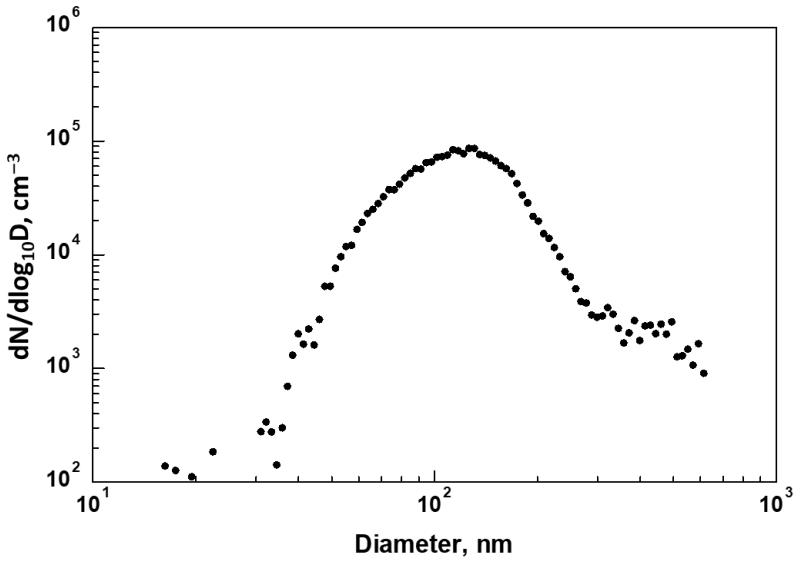

Figure S1: Example particle size distribution generated by the TSI 9302 Single Jet Atomizer.

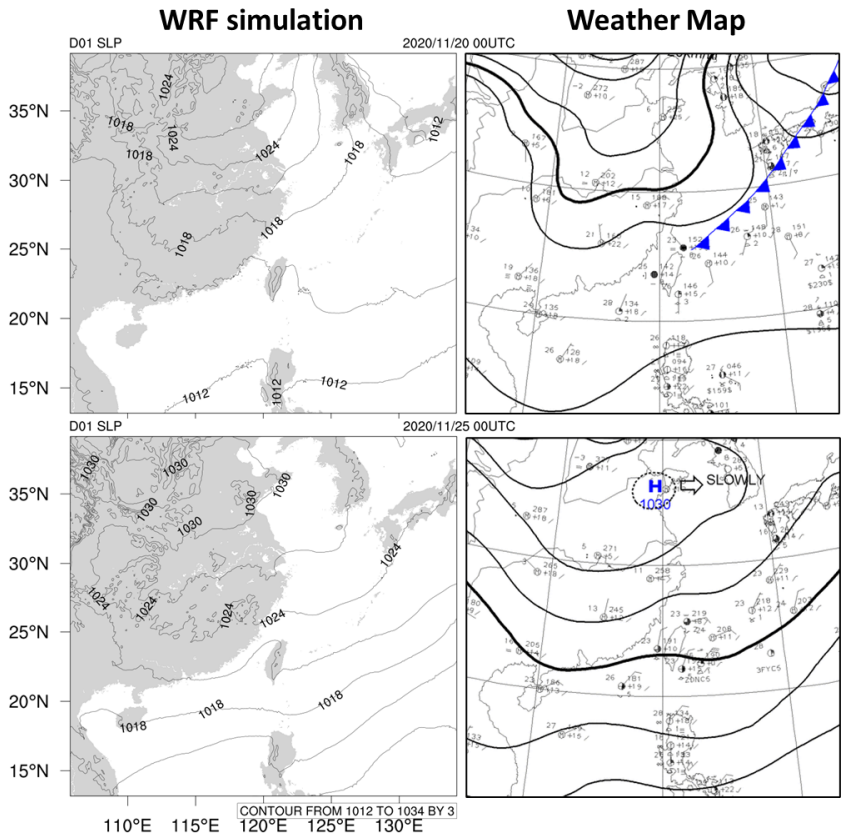

Figure S2: Simulated surface pressure fields in Domain 1 (left) and the corresponding surface weather maps (right) for the events on 20 November 2020 (top) and 25 November 2020 (bottom).

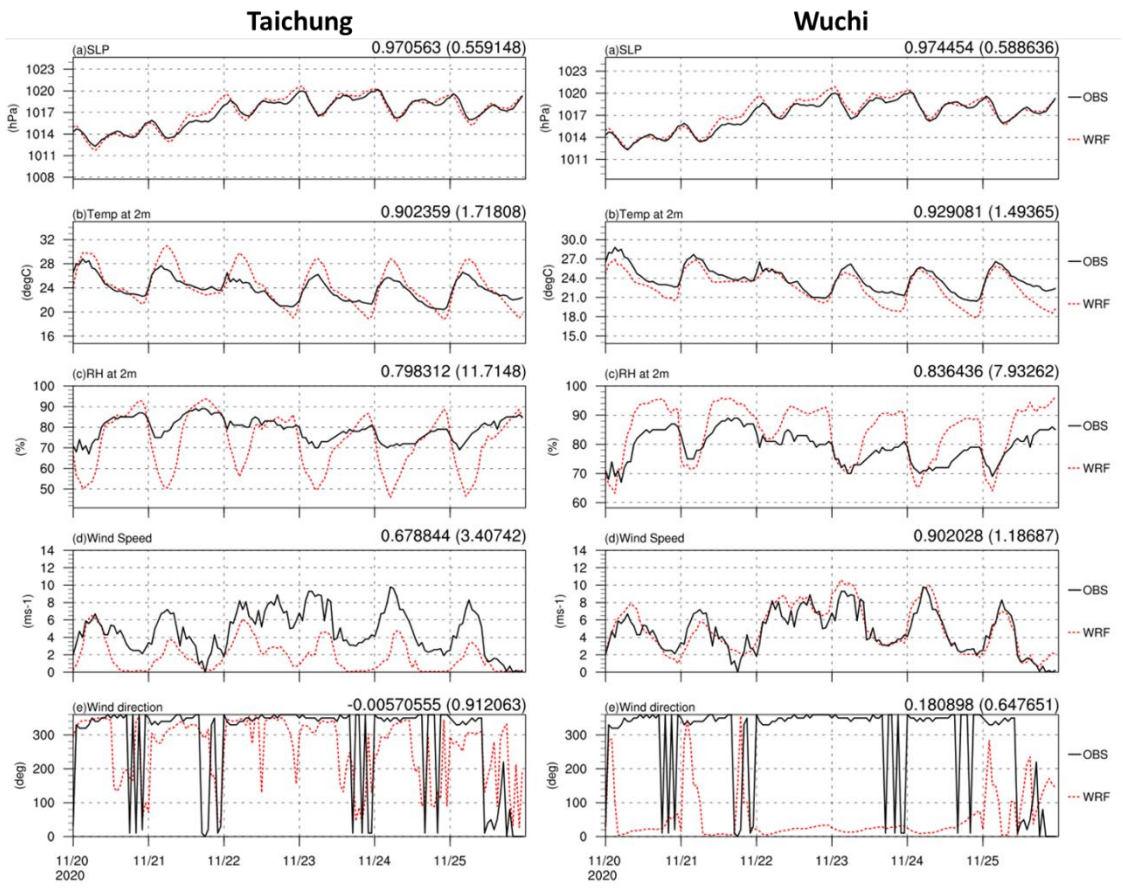

Figure S3: Comparison of simulated (red-dotted lines) and observed (black lines) meteorological parameters at two weather stations near the PNC measurement site at Xitun. Left: Taichung station (24.1458° N, 120.6841° E); right: Wuchi station (24.2560° N, 120.5234° E). Meteorological parameters shown from top to bottom are sea-level pressure, 2-m air temperature, 2-m relative humidity, 10-m wind speed, and 10-m wind direction.

The comparisons in Figs. S2 and S3 indicate that the meteorological simulations exhibit some biases; however, their magnitudes are comparable to those typically reported in routine weather forecasts by our meteorological agency.

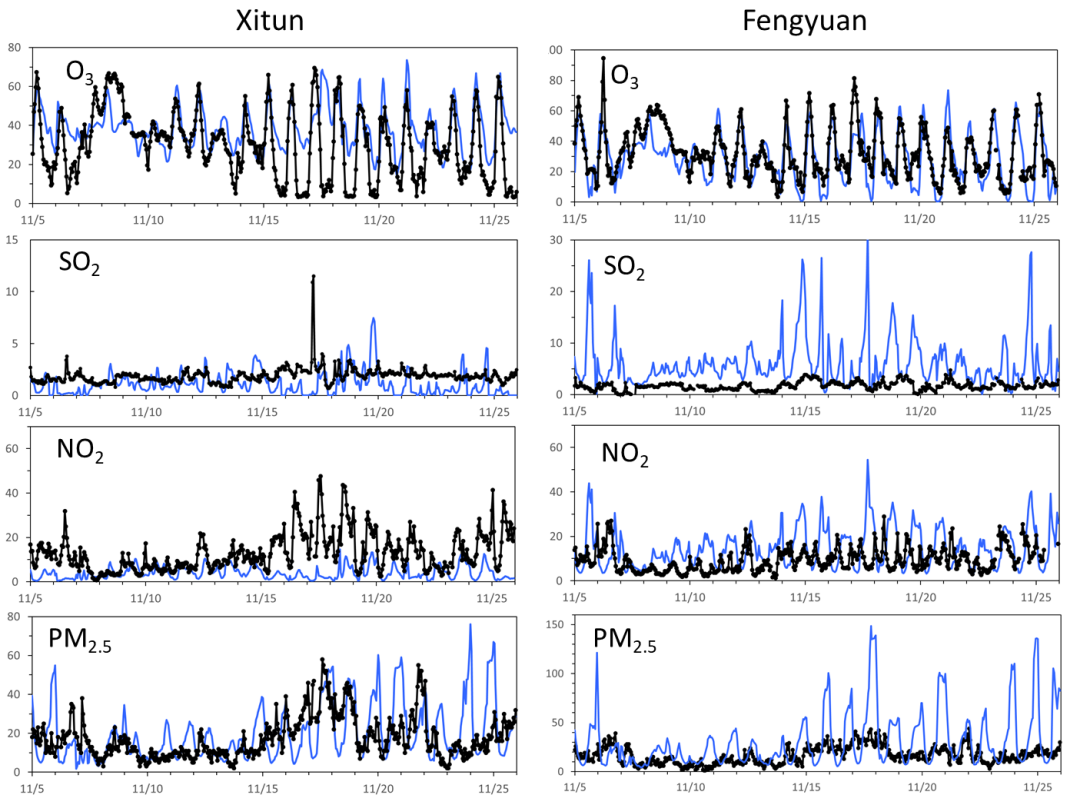

Figure S4: Observed (black lines) and simulated (blue lines) precursor gas concentrations at Xitun and Fengyuan. Concentrations of all species are reported in ppb.

Overall, simulated NO_2 concentrations are generally lower than those observed at the Xitun station. In addition to uncertainties in the meteorological fields, a likely contributing factor is the treatment of emissions in CMAQ, which spatially distributes point and line sources over the 2 × 2 km grid, thereby smoothing sharp near-road concentration gradients. This effect is particularly pronounced at Xitun, which is located in a dense urban environment adjacent to major roads and highway interchanges. In contrast, biases in simulated NO_2 are smaller at the Fengyuan station, which lies in a transitional zone between the urban core of Taichung and the more rural northeastern region and is therefore less directly influenced by intense traffic emissions.

Simulated SO_2 concentrations at Xitun are of the correct order of magnitude; however, the observed time series exhibits weaker temporal variability. This discrepancy suggests that the model may underestimate background SO_2 levels while overestimating the influence of nearby point sources, such as the industrial park and power plant. This tendency is even more pronounced at the Fengyuan station.

The simulated O_3 concentrations show better overall agreement with observations, but exhibit notable nighttime overestimation, especially at Xitun. This bias is likely related to insufficient NO titration when NO emissions are instantaneously diluted over a model grid cell. Unfortunately, routine observations of $PM_{2.5}$ chemical composition were not available during the study period, preventing a more detailed evaluation of individual $PM_{2.5}$ components. The root-mean-square error of the simulated SO_2, NO_2 and O_3 concentrations are 1.6, 12.5, and 16.7 ppb, respectively.

For $PM_{2.5}$, the most evident discrepancy is nighttime overestimation, especially during the latter half of November. This bias is attributable to an overly shallow nocturnal planetary boundary layer, which suppresses vertical mixing—a known limitation in CMAQ applications over the study region. In addition, during November 15–19 the model persistently underestimates daytime $PM_{2.5}$ (more noticeably at Xitun). This underestimation may be associated with leeside vortex

formation over western Taiwan under prevailing easterly flow, which can recirculate pollutants that have been transported offshore; this recirculation was likely not well captured by the model.

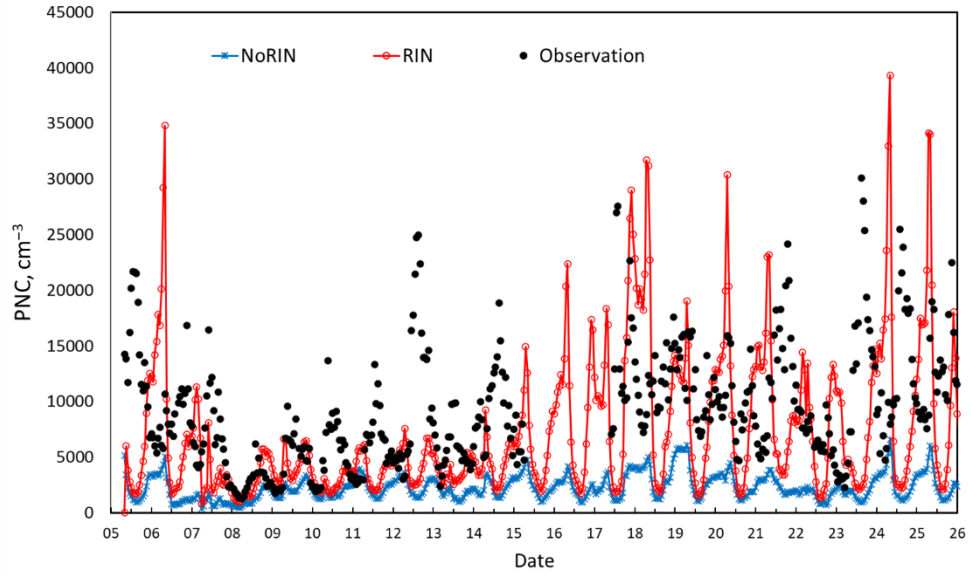

Figure S5. Time series of simulated particle number concentration (PNC) from the NoRIN (blue line) and $RIN_{D\sigma}$ (red line) scenarios, together with observations (black line), for the full simulation period in November 2020. The NoRIN simulation consistently underestimates PNC, whereas the $RIN_{D\sigma}$ simulation shows substantial improvement, particularly during late November. The root-mean-square error (RMSE) is 8771 for NoRIN and 8148 for $RIN_{D\sigma}$. Results from other RIN scenarios fall between the NoRIN and $RIN_{D\sigma}$ cases and are omitted for clarity.

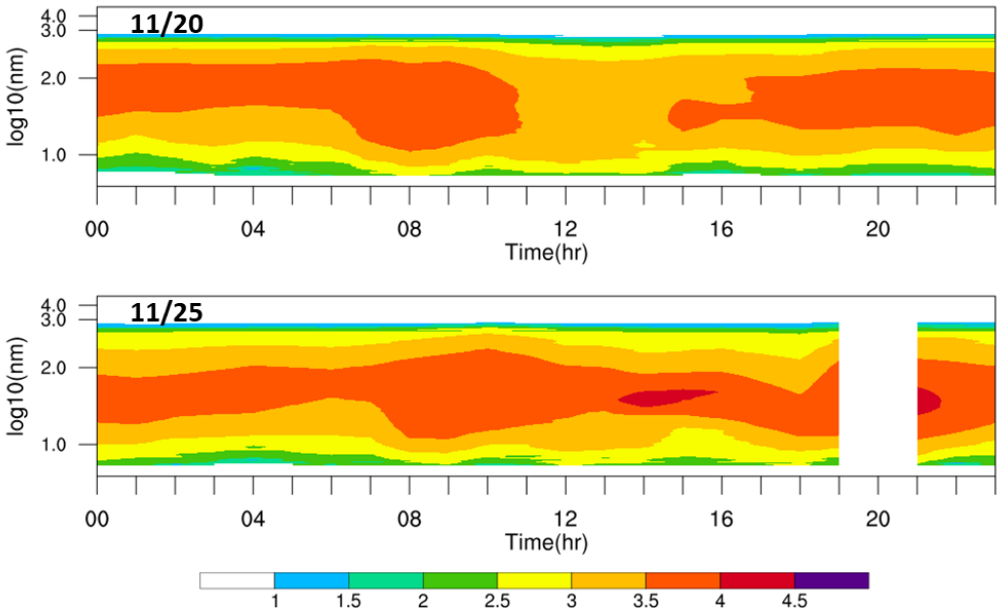

Figure S6. Temporal evolution of the particle number size distribution (dN/dlogD) observed at Xitun on 20 November (top) and 25 November (bottom) 2020. The abscissa shows local time (hours), and the ordinate shows particle diameter (nm, logarithmic scale). The color bar indicates number density (dN/dlogD; cm^{-3}) on a base-10 logarithmic scale, with null values masked.

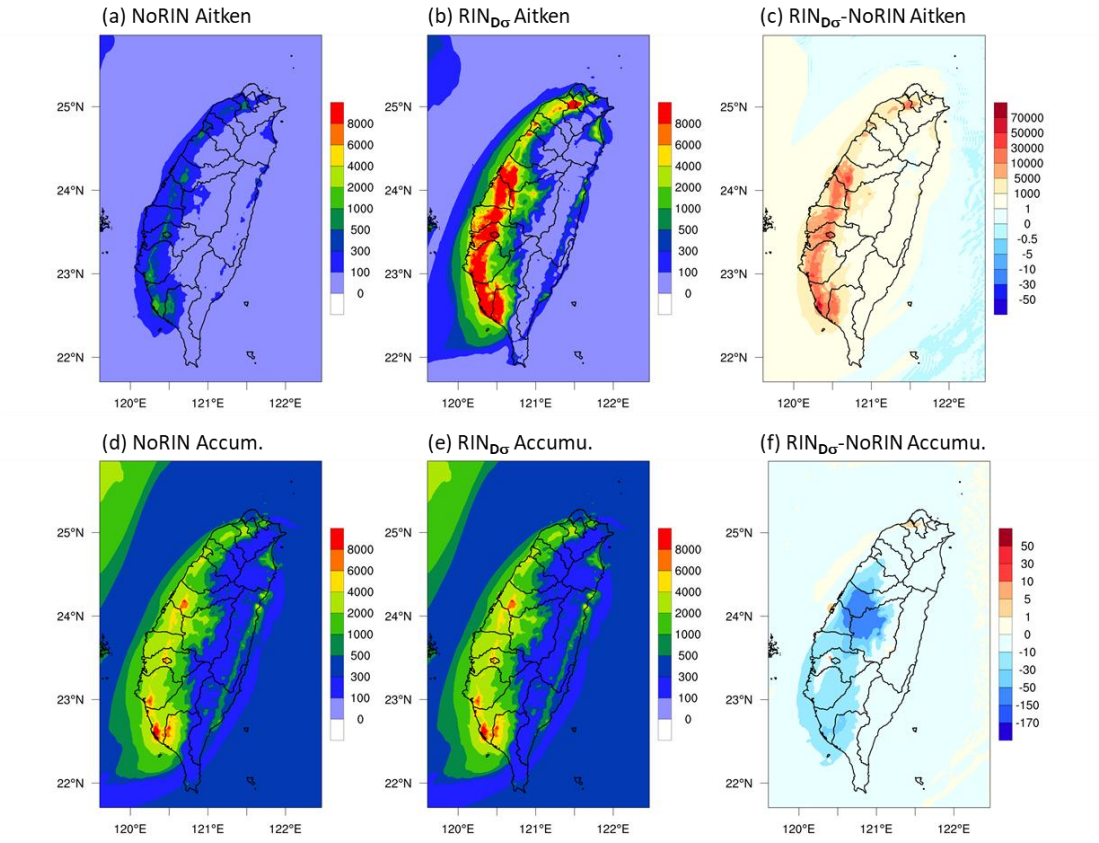

Figure S7: Same as Figure 8, but for the data of 25 November 2020.